# POTENTIAL OF DIRECTIONALLY SOLIDIFIED EUTECTIC CERAMICS FOR HIGH-TEMPERATURE APPLICATIONS

M. Parlier*, R. Valle*, L. Perrière*,**, S. Lartigue-Korinek**, L. Mazerolles**
*ONERA/DMSC, 29 avenue de la Division Leclerc, F-92322 Châtillon, France
**ICMPE-MCMC, UMR 7182, CNRS–Univ. Paris Est, 2-8 rue H. Dunant, F-94320 Thiais, France

## ABSTRACT

Directionally solidified eutectic (DSE) ceramics add new potentialities to the advantages of sintered ceramics: a higher strength almost constant up to temperatures close to the melting point and a better creep resistance. The microstructure of melt growth composites (MGC) of ceramic oxides consists in three-dimensional and continuous interconnected networks of single-crystal eutectic phases. After solidification of binary eutectics, the eutectic phases are alumina and either a perovskite or garnet phase. In ternary systems, zirconia is added as a third phase. The present investigation is focused on both binary ($Al_2O_3$-$Y_3Al_5O_{12}$ (YAG), $Al_2O_3$-$Er_3Al_5O_{12}$ (EAG) and $Al_2O_3$-$GdAlO_3$ (GAP)) and ternary ($Al_2O_3$-YAG-$ZrO_2$, $Al_2O_3$-EAG-$ZrO_2$ and $Al_2O_3$-GAP-$ZrO_2$) eutectics. Improving the strength and toughness of DSE ceramics being essential for practical applications such as turbine blades in future aerospace engines or thermal power generation systems, results concerning the mechanical behaviour of these eutectics will be reported after a short presentation concerning microstructure and crystallography. This better knowledge of DSE ceramics has led to the development of a specific Bridgman furnace to produce large crystals and turbine blades.

## INTRODUCTION

The development of new ultra high temperature structural materials in the aerospace field and in particular for gas turbine applications is a real challenge nowadays. In fact, the use of superalloys at temperatures beyond 1150°C will be difficult despite the various studies performed to increase their heat-resistance.

For higher temperatures, sintered ceramic oxides offer many advantages compared to nickel-based superalloys: resistance to oxidation and abrasion, lower density. Unfortunately, sintered ceramics are brittle and failure strength decreases when the temperature increases. Ceramic materials prepared by unidirectional solidification of oxides from the melt add new potentialities to the advantages of sintered ceramics: a higher strength almost constant up to temperatures close to the melting point (no secondary phase at the grain boundaries), good creep resistance, stability of the microstructure and no chemical reaction between the constituent phases [1, 2]. Recently, studies on eutectic compositions between alumina and rare-earth oxides led to microstructures consisting of two entangled phases in a three-dimensional and continuous network. After solidification, the eutectic phases are alumina and either a perovskite phase $LnAlO_3$ (Ln: Gd, Eu) or a garnet phase $Ln_3Al_5O_{12}$ (Ln: Y, Yb, Er, Dy). In the case of ternary systems, zirconia was added to promote toughness.

Studies to control the microstructure of directionally solidified eutectic (DSE) ceramics have been performed, acting on the processing parameters of the floating-zone method (arc image furnace). The mechanical properties have thus been investigated on the small specimens manufactured through this process. With the aim to understand the toughening mechanisms, a biaxial testing disc flexure device has been used to investigate the propagation of cracks in the various phases and in the interfaces. These observations have been correlated to internal stress calculations and spectroscopic measurements. Moreover, the high performance creep behaviour at high temperature (1450-1600°C) has been determined using compression tests. It has been demonstrated that creep mechanisms evolve with the macroscopic thermomechanical loading (temperature, stress) and correlation has been established with the entangled microstructure [3-9].

The next step has been devoted to establish the feasibility of larger crystals using the Bridgman method that is more appropriate to obtain a homogeneous microstructure. A specific directional solidification furnace has been developed to produce crystals with melting temperatures up to 2200°C and demonstrate the possibility of direct solidification of turbine blades.

## MICROSTRUCTURE AND CRYSTALLOGRAPHY

### *Microstructure*

Under controlled conditions, solidification from the melt leads to materials free of porosity and with only a very few grain boundaries which are generally at the origin of brittleness in sintered ceramics. Furthermore, directional solidification often results in highly textured materials with well-defined crystallographic orientation relationships between the constituent phases. The equipments used for the growth of oxide–oxide eutectics are high temperature single-crystal growth devices displaying a high thermal gradient. In the present case, rods of oriented eutectics, about 8 mm in diameter, were grown using the floating-zone translation technique. Solidification runs were achieved in an arc image furnace operating with a 6 kW xenon lamp as a radiation source, at various rates, ranging from 2 to 30 mm $h^{-1}$.

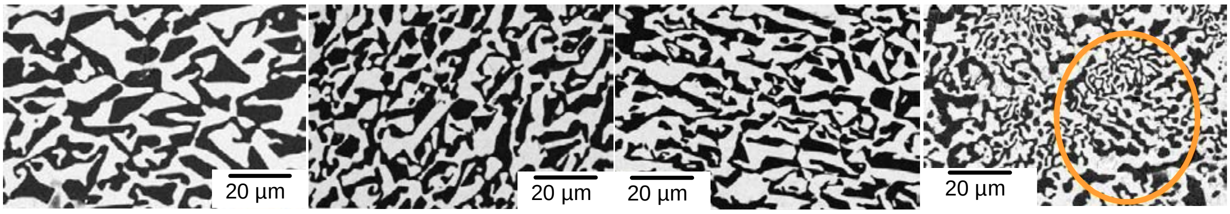

(a) (b) (c) (d)

Fig. 1. Back-scattered SEM micrographs of the $Al_2O_3$–YAG ($Y_3Al_5O_{12}$) eutectic composite ($Al_2O_3$: dark contrast). Morphology of microstructure *vs.* the solidification rate: 5 mm/h (a), 12 mm/h (b), 20 mm/h (c) and 30 mm/h (d).

In most directionally solidified oxide eutectics, coupled growth is mainly controlled by the growth rate. When this rate increases the eutectic growth undergoes a transition from the planar to the cellular regime that does not correspond anymore to a coupled growth. Scanning Electron Microscopy (SEM) images (Fig. 1) reveal that the three-dimensional microstructure of the $Al_2O_3$–YAG eutectic is slightly modified when the growth rate increases; it becomes finer (Fig. 1c) and persists up to rates close to 30mm$h^{-1}$, before entering into the cellular growth regime (Fig. 1d). Similar results were obtained with the other eutectic compositions, thus leading to a selected growth rate of 10 mm$h^{-1}$.

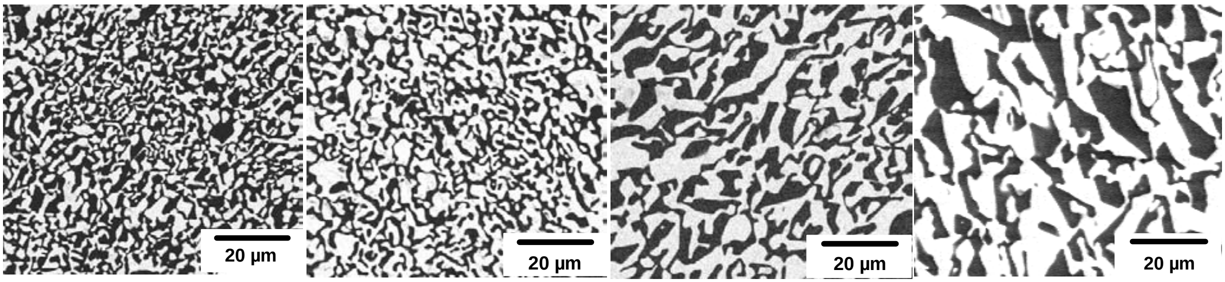

(a) (b) (c) (d)

Fig. 2. Back-scattered SEM micrographs of the transverse sections of binary eutectics showing the continuous three-dimensional interconnected microstructure consisting of $Al_2O_3$ (dark contrast) and single-crystal: GAP = $GdAlO_3$ (a), EAG= $Er_3Al_5O_{12}$ (b), YAG = $Y_3Al_5O_{12}$ (c) or DAG = $Dy_3Al_5O_{12}$ (d).

SEM images of the microstructures corresponding to cross-sections perpendicular to the solidification direction are shown in Fig. 2. In each case, continuous networks of two single-crystal phases are observed: $Al_2O_3$ (dark contrast) and a perovskite (P) or garnet (G) phase (bright contrast). The same morphology was observed on sections parallel to the growth direction, thus revealing the three-dimensional configuration of the microstructure in these systems. The two phases interpenetrate without grain boundaries, pores or colonies. The domain mean size of each phase (length of the shortest axis) is similar for the $Al_2O_3$-GAP and $Al_2O_3$-EAG eutectics (Fig. 2a, b), whereas it is much larger for the $Al_2O_3$–YAG and $Al_2O_3$–DAG eutectic composites. Moreover, the $Al_2O_3$-GAP and $Al_2O_3$-EAG eutectics exhibit curved interfaces; on the contrary, the $Al_2O_3$–YAG and $Al_2O_3$–DAG eutectics display a faceted microstructure with large planar interfaces (Fig. 2c, d).

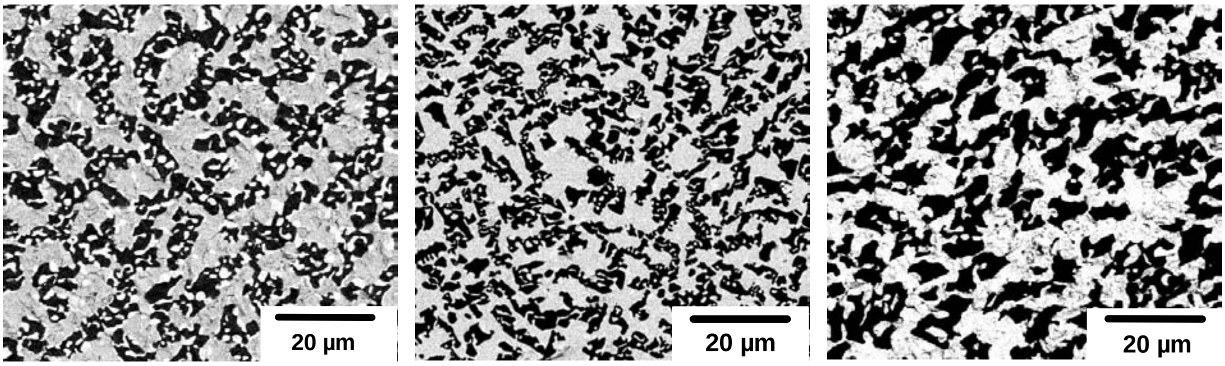

(a) (b) (c)

Fig. 3. Back-scattered SEM micrographs of the transverse sections of ternary eutectics containing $Al_2O_3$ (dark contrast), YAG (a), EAG (b) and GAP (c) and zirconia (bright contrast dots).

Typical microstructures of transverse sections of ternary eutectics are shown in Fig. 3. First of all, it should be noted that morphology of the garnet-type phase (YAG or EAG) is modified depending on the rare-earth oxide added to alumina and zirconia. At the same solidification rate, large facets are developed in the $Al_2O_3$-EAG-$ZrO_2$ ternary eutectic (Fig. 3b), contrary to the $Al_2O_3$-YAG-$ZrO_2$ ternary eutectic (Fig. 3a). Secondly, the $Al_2O_3$-YAG-$ZrO_2$ ternary eutectic displays a fine microstructure with curved smooth interfaces, instead of the coarser microstructure with large planar interfaces and sharp angles observed in the $Al_2O_3$–YAG binary eutectic (Fig. 2c). In the $Al_2O_3$-YAG-$ZrO_2$ ternary eutectic, zirconia phase always grows at the interface between $Al_2O_3$ and YAG. In the case of $Al_2O_3$-EAG-$ZrO_2$ and $Al_2O_3$-GAP-$ZrO_2$ ternary eutectics, cubic zirconia dispersoids are observed, not only at the interfaces, but also in the alumina phase (more clearly evidenced at a higher magnification, in Fig. 5, reporting crack propagation modes in ternary eutectics).

### ***Crystallography***

Aligned eutectic microstructures (lamellae, fibres …), grown by unidirectional solidification, usually consist of single-crystal phases growing preferentially along well-defined crystallographic directions. These directions are not necessarily the directions of easy-growth of the isolated components but often correspond to minimum interfacial energy configurations between phases. These perfectly aligned lattices are related by orientation relationships which are unique in most systems and produce well-defined interface planes corresponding to dense atomic arrangements in the component phases. Although the DSE do not display 1-D or 2-D aligned microstructures, but 3-D interconnected microstructures, electron diffraction studies performed in Transmission Electron Microscopy (TEM) on thin plates cut perpendicularly to the solidification axis reveal growth directions also corresponding to well-defined crystallographic directions (Table 1).

| Eutectic phases | $Al_2O_3$-LnAP (perovskite) | $Al_2O_3$-LnAG (garnet) |
|---|---|---|
| Growth directions | $[10\bar{1}0]$ $Al_2O_3$ // [110] LnAP | $[10\bar{1}0]$ $Al_2O_3$ // [110] LnAG |
| Orientation relationships | $(2\bar{1}\bar{1}0)$ $Al_2O_3$ // (001) LnAP | (0001) $Al_2O_3$ // $(1\bar{1}2)$ LnAG |

Table 2. Growth directions and orientation relationships of the directionally solidified eutectic composites.

These results, obtained from Selected Area Electron Diffraction (SAED) patterns correspond to analyzed regions of a few micrometers in size; in order to control the single-crystal homogeneity over larger areas, the Electron BackScattered Diffraction (EBSD) technique was used. Fig. 4 shows the Pole Figures and the Inverse Pole Figure (IPF) maps for the $Al_2O_3$–YAG eutectic ceramics. The orientation maps presented in Fig. 4 reveal the sample texture and the nearly single crystal homogeneity of the sample. Each colour corresponds to one crystallographic direction as indicated in the reference stereographic triangles. For example (Fig. 4a, bottom), YAG crystals with their $\langle 111 \rangle$ axis normal to the surface of the sample would be blue, and so on. A unique colour corresponds to the YAG phase which thus exhibits only one growth direction. Two different colours are visible for alumina (Fig. 4a, top); however, the $[10\bar{1}0]$ and $[01\bar{1}0]$ growth directions correspond to the same $\{10\bar{1}0\}$ orientation (two twin-related variants of $Al_2O_3$). Moreover, the pole figures (Fig. 4b) reveal an orientation relationship between the two phases: $(0001)_{Al2O3}$ // $(1\bar{1}2)_{YAG}$.

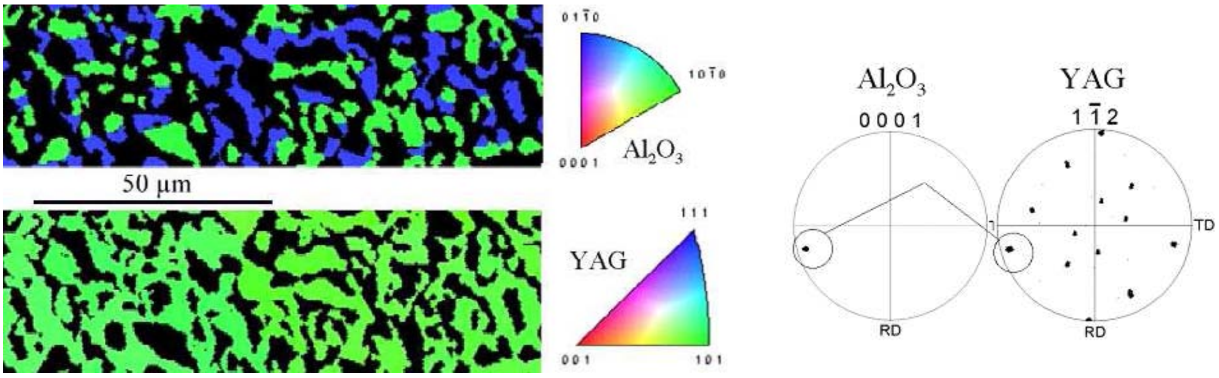

(a)

(b)

Fig. 4. Inverse Pole Figure maps of $Al_2O_3$ and YAG phases (a) and Pole Figures of $0001_{Al2O3}$ and $112_{YAG}$ orientations (b). Orientation relationship: $(0001)_{Al2O3}$ // $(1\bar{1}2)_{YAG}$ (b).

Concerning the interfaces between corundum, perovskite, garnet and zirconia, atomic scale High Resolution Transmission Electron Microscopy (HRTEM) investigations have revealed the absence of an interphase layer [1, 2, 8]. The orientation of the interface with respect to the adjacent phases growing in epitaxy and the mismatch between the lattice parameters result in a regular network of intrinsic defects. However, in each phase, the stress field resulting from such an interface is so local and so faint that it cannot be detected in conventional TEM, thus assessing a minimum energy configuration of the interfaces.

## MECHANICAL PROPERTIES

### *Crack nucleation and propagation modes*

Improving the strength and toughness of eutectic ceramics requires a better knowledge of the crack propagation modes in such an interconnected microstructure. In this respect, a biaxial disc flexure testing device has been designed and built at Onera [7]. In the six investigated directionally solidified eutectics, the essential propagation mode is transgranular crack propagation (Fig. 5). A zig-zag crack growth with multiple branches is observed in most cases. However, this type of crack propagation does not only result from deflections of the cleavage crack inside each phase or when crossing phase boundaries, but more essentially from crack deflection in the interfaces themselves. Interface crack propagation is thus observed between $Al_2O_3$ and YAG (large black arrows in Fig. 5 a), $Al_2O_3$ and EAG (large black arrows in Fig. 5 b), $Al_2O_3$ and GAP (large black arrows in Fig. 5 c), $Al_2O_3$ and $ZrO_2$ (white arrows in Fig. 5 a, b and c), YAG and $ZrO_2$ (sharp black arrow in Fig. 5 a) and EAG and $ZrO_2$ (sharp black arrow in Fig. 5 b). However, interface crack propagation is not observed between GAP and $ZrO_2$. Crack branching is observed, not only in one of the various phases such as $ZrO_2$ (split arrow in Fig. 5 a), but also in the interfaces where crack deflection through debonding has occurred (split arrows in Fig. 5 c). In most cases, these bifurcation mechanisms lead to stopped cracks (Fig. 5 a and c).

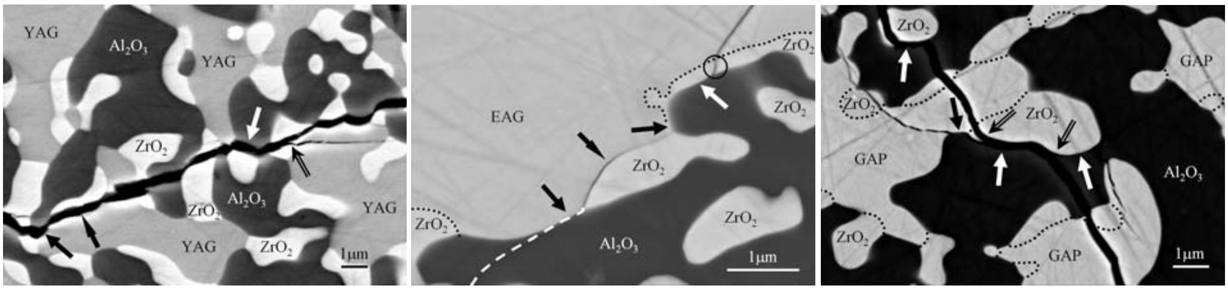

(a) (b) (c)

Fig. 5. Crack propagation modes at room temperature in ternary eutectic ceramics subjected to biaxial flexure (FEG-SEM, back-scattered electrons): $Al_2O_3$-YAG-$ZrO_2$ (a), $Al_2O_3$-EAG-$ZrO_2$ (b) and $Al_2O_3$-GAP-$ZrO_2$ (c).

The various crack propagation modes may be correlated to internal thermal stress measurements and calculations. For instance, the presence of $ZrO_2$ phases surrounded by a continuous layer of $Al_2O_3$ (Fig. 5 b (top right corner) and c (top left corner)) suggests the use of a concentric cylinder model (Fig. 6 a). For instance, the $ZrO_2$ phases in Fig. 5 b (top right corner) and c (top left corner) may be represented by a 1 µm in diameter $ZrO_2$ bar, bonded into a 1.5 µm thick $Al_2O_3$ sleeve, surrounded by a 0.5 µm thick $ZrO_2$ sleeve, these three concentric cylinders being embedded into an equivalent homogeneous medium (EHM) having the diameter of the specimen under investigation and the macroscopic thermo-mechanical properties of the bulk $Al_2O_3$-EAG-$ZrO_2$ or $Al_2O_3$-GAP-$ZrO_2$ eutectics, respectively. In the case of the $Al_2O_3$-GAP-$ZrO_2$ eutectics, subjected to a temperature change ($\Delta T \approx 1700$ °C), the normal stress ($\sigma_n$) acting on the $ZrO_2$-$Al_2O_3$ interface attains $\approx 1000$ MPa (Fig. 6 b); this high tensile normal stress helps interface crack propagation, as observed in Fig. 5 c (top left corner). The external $ZrO_2$ layer is subjected to a high tensile circumferential loading ($\sigma_\theta \approx 1800$ MPa) which helps transgranular crack propagation in these phases, as observed in Fig. 5 b (circle, top right corner) and c (top left corner). As compared to the ultimate tensile strength of such eutectic ceramics [2, 10], the level of these internal thermal stress components is very high, which may explain their essential role in crack nucleation and propagation e.g. the possibility of crack deflection in the interfaces in the ternary eutectic ceramics. The fact that the observed crack deflection modes are more numerous in ternary than in binary eutectics is in good agreement with the fact that the fracture toughness is improved from the individual constituents to the binary eutectics (≈ 7 MPa m½) and to the ternary eutectics (≈ 10 MPa m½) [4, 5].

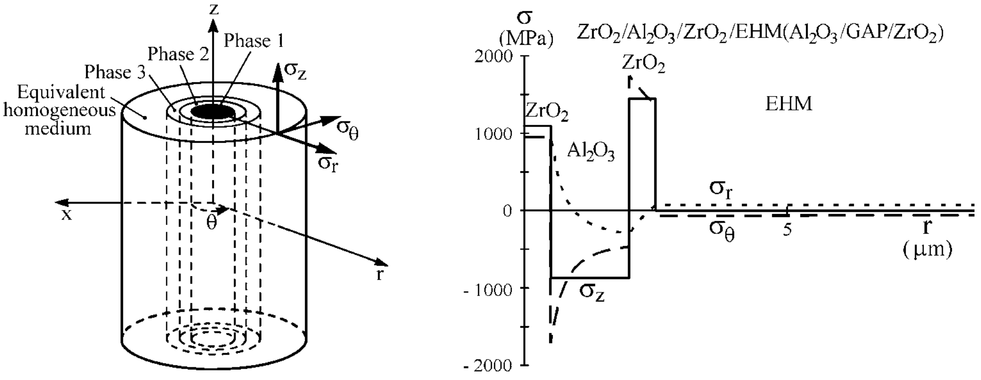

(a) (b)

Fig. 6. Internal thermal stresses. The four-phase concentric cylinder model (a) and the corresponding stress system (b), where $\sigma_n$ is given by the radial stress component $\sigma_r$.

### *Compressive creep behaviour*

The compressive creep tests performed on the binary and ternary eutectics under consideration were conducted in air within the stress range 50 to 200 MPa and the temperature range 1450 to 1600°C. The major axis of the parallelepipedic compressive creep specimens was parallel to the solidification direction.

The creep deformation curves show a primary creep regime where the deformation rate decreases continuously. After this short primary stage (e.g. strain of about 0.5%), the secondary creep rate is reached [8, 9]. The secondary creep rate $\dot{\varepsilon}$ is very sensitive to the applied stress σ, following a power–law relationship

$$\dot{\varepsilon} = A\sigma^{n} \exp - Q/RT$$

where A is a material constant, n, the stress exponent, Q, the activation energy for creep, R, the gas constant and T, the absolute temperature.

Determination of the stress exponent, n, and of the activation energy, Q, allows identifying the creep mechanisms responsible of the creep behaviour of the eutectic composites. These quantities are given by

$$n = \left.\frac{\partial \ln \dot{\varepsilon}}{\partial \ln \sigma}\right)_T \qquad \text{and} \qquad Q = \left.\frac{\partial \ln \dot{\varepsilon}}{\partial 1/T}\right)_\sigma$$

Consequently, tests performed at a given temperature, with load increments or decrements, will allow the determination of n, whereas tests performed under a given loading, with temperature increments or decrements, will allow the determination of Q. In both cases, increments or decrements are applied once a steady-state regime is attained and the strain rate, corresponding to each step, experimentally determined [9]. Although the eutectics under consideration have been thoroughly tested under compressive creep [9], only the more representative results will be reported in the present paper (Fig. 7).

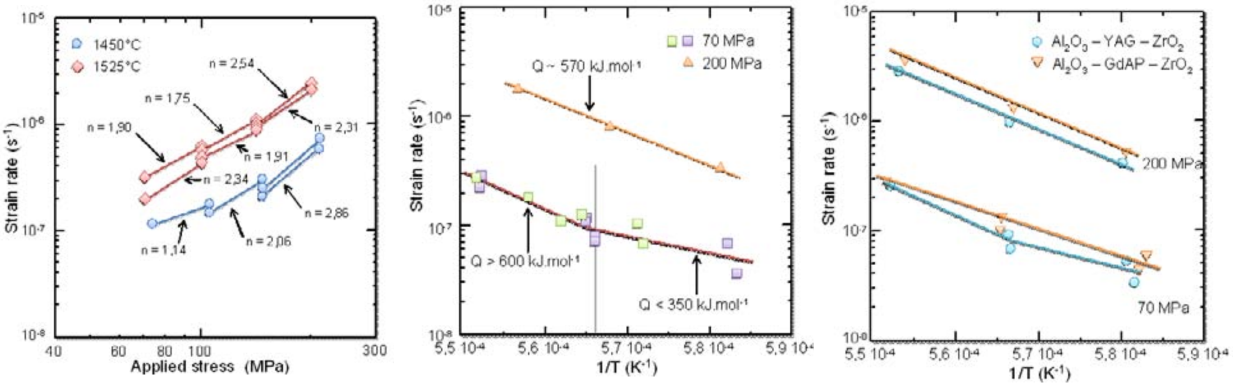

(a) (b) (c)

Fig. 7. Compressive creep tests. Creep strain rate *vs*. applied stress at 1450°C and 1525°C for the $Al_2O_3$-YAG eutectic (a). Creep strain rate *vs*. temperature (1/T) under 70 and 200 MPa loadings for the $Al_2O_3$-EAG eutectic (b). Creep strain rate *vs*. temperature (1/T) under 70 and 200 MPa loadings for the $Al_2O_3$-YAG-$ZrO_2$ and $Al_2O_3$-GAP-$ZrO_2$ eutectics (c).

From the results reported in Fig. 7a, it should be noted that, at 1450°C, the stress exponent (n) increases more rapidly, as the applied stress is increased, than at 1525°C. Under a low applied stress, a value of n such as 1.14 corresponds to a creep strain rate nearly proportional to the applied stress. Such a value of n suggests a diffusion controlled creep mechanism. At a high stress level and/or high temperature, the value of n is higher ($2<n<3$), which suggests creep mechanisms controlled by dislocation motion.

Concerning the activation energy of $Al_2O_3$-Garnet eutectics (Fig. 7b), the value of $Q \approx 350$ kJ/mol is determined only for temperatures lower than 1490°C and under a low applied stress (70 MPa); the activation energy is otherwise higher: $Q \approx 600$ kJ/mol. Such a high value of Q may correspond to self-diffusion of oxygen atoms either in the garnet or in the alumina phase [11].

In the case of ternary eutectics, the variation of n as a function of the applied stress is similar to that determined in the binary eutectics [9]. Concerning the activation energy (Fig. 7c), the value of $Q \approx 400$ kJ/mol is also found for a temperature lower than ≈ 1500°C in the only case of $Al_2O_3$-YAG-$ZrO_2$, a behaviour which is similar to that observed in the binary $Al_2O_3$-Garnet eutectics (Fig. 7b). In the other conditions, an activation energy of $Q \approx 600$ kJ/mol has been determined. Concerning the creep strain rates of the ternary eutectics, it should be noted that the behaviour of the $Al_2O_3$-YAG-$ZrO_2$ and $Al_2O_3$-GAP-$ZrO_2$ eutectics is similar to that of the corresponding binary eutectics whereas that of the $Al_2O_3$-EAG-$ZrO_2$ eutectic is lower [9].

TEM studies were performed on specimens previously subjected to compressive creep tests. Due to the strong interface bonding between the various phases, interface sliding mechanisms are impossible. Moreover, due to the difficulty for dislocations to cross the interfaces (difference in lattice parameters), the only possibility to transmit plastic deformation from one phase to the other is to activate a dislocation source in one phase, under the stress concentration resulting from the presence of a dislocation pile-up in the other phase. Otherwise, both phases must deform independently in order to accommodate the global creep deformation. In each phase, the gliding dislocations have to bow within the phase width ($\lambda$). The shear stress $\tau$ necessary for this process is given by

$$\tau = G\mathbf{b}/\lambda$$

where G is the shear modulus and **b** the Burgers vector.

Consequently, when the size of microstructure decreases (e.g. eutectic morphologies reported in Fig. 2), the activation of dislocation glide requires higher stresses.

In alumina (Fig. 8a), the observed dislocations are basal type dislocations ($b = 1/3\,[2\bar{1}\bar{1}0]$) aligned in parallel (0001) basal slip planes. This is in agreement with the fact that the basal slip system has the lowest critical resolved shear stress at high temperature. A dislocation pile-up has also been observed in the GAP phase (Fig. 8b). This pile-up interacts with the GAP–alumina interface at the bottom of the image, and a basal twin is seen in alumina close to the interaction. Mechanical twinning is probably due to accommodation of the stress concentration resulting from the pile-up. Dislocations are present in the twin boundaries. It is worth noting that usually large stresses are necessary to activate basal twins. Only in a few cases, basal twinning has been observed in alumina submitted to plastic deformation. These observations are in agreement with the high value of the applied stress.

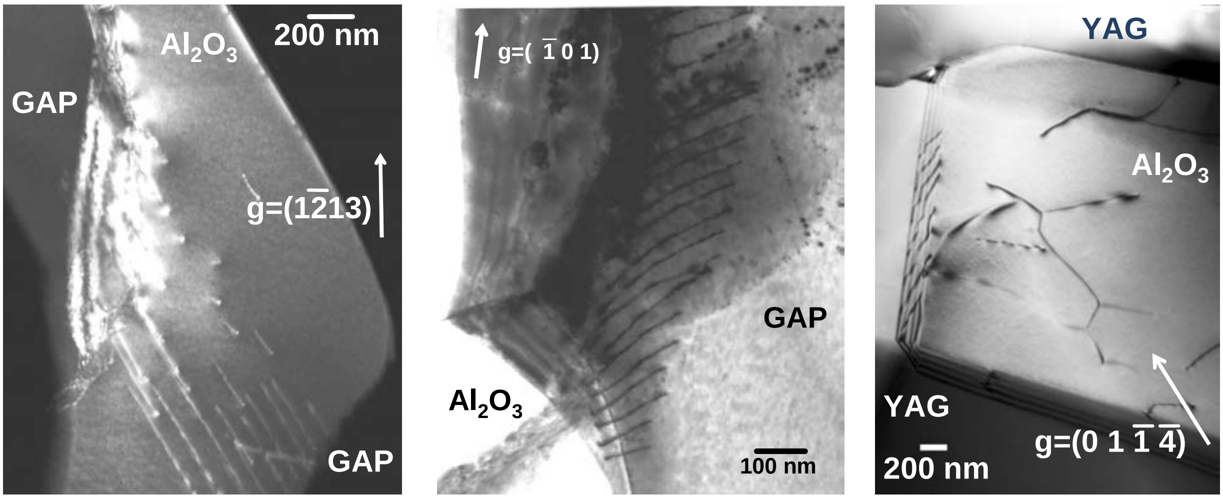

(a) (b) (c)

Fig. 8. TEM examinations of compressive tested specimens. Dislocation glide in the $Al_2O_3$ phase of a $Al_2O_3$-YAG eutectic (a). Dislocation pile-up in the GAP phase of a $Al_2O_3$-GAP eutectic (b). Dislocation reaction involving climb in the $Al_2O_3$ phase of a $Al_2O_3$-YAG eutectic (c).

Thermally activated mechanisms such as dislocation climb have also been observed (Fig. 8c). Such a dislocation network, resulting from the reaction of dislocations from the basal and pyramidal slip systems, involves dislocation climb. This diffusion controlled deformation mode was observed in an $Al_2O_3$-YAG specimen previously subjected to a creep test for which an activation energy of $Q \approx 670$ kJ/mol was determined.

The TEM examinations have evidenced plastic deformation of the various phases; furthermore, the different deformation modes thus observed are in good agreement with the stress exponents and activation energies experimentally determined.

## FEASIBILITY OF TURBINE BLADES IN A LARGE BRIDGMAN FURNACE

A large Bridgman furnace has been manufactured (Cyberstar, Grenoble, France) according to the specifications established by Onera (Fig. 9). This device which includes two superposed radiofrequency heating elements ensures a melting zone temperature up to 2200°C (±1°C) and a crystallization zone temperature up to 1600°C (±1°C). In the liquid/solid transition zone, a thermal gradient between 20°C/cm and 40°C/cm is attained. This Bridgman furnace operates either under vacuum or neutral atmosphere up to

15 bars and allows a growth rate from 5 to 50 mm/h. The molybdenum crucible allows the directional solidification of large eutectic crystals up to 50 mm in diameter and 200 mm in height.

Studies in progress concern the determination of the solidification parameters in order to optimize the microstructure of the $Al_2O_3$/GAP and $Al_2O_3$/YAG/$ZrO_2$ eutectics and their thermo-mechanical characterization e.g. flexural strength up to 1500°C. New eutectic compositions without $Al_2O_3$ phase will be also investigated to improve the resistance to high temperature water vapor corrosion. Finally, the feasibility of the elaboration of near net shape turbine blades will be investigated.

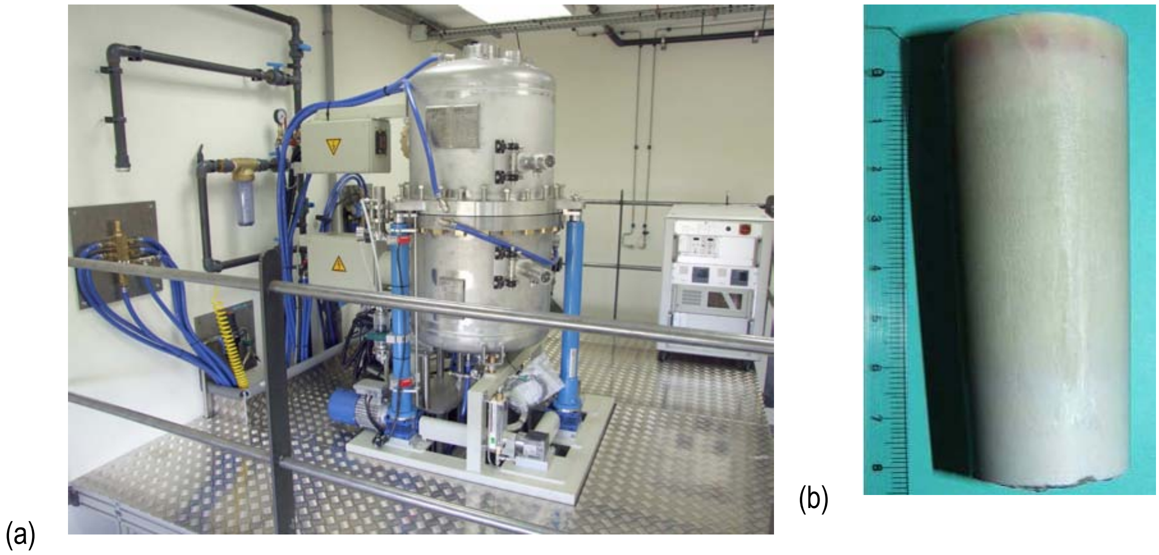

Fig. 9. The Bridgman furnace (a) and a large $Al_2O_3$/$GdAlO_3$ crystal obtained using this furnace (b).

## CONCLUSION

Ceramic materials prepared by unidirectional solidification of oxides from the melt are under investigation at Onera for applications in the aerospace field and in particular for gas turbine blades. Studies to control the microstructure of the directionally solidified eutectic ceramics have been performed and the mechanical properties have been investigated with the aim to understand the toughening mechanisms and the creep behaviour at high temperature. In the ternary eutectic ceramics, the high level of the internal thermal stresses may explain their essential role in crack nucleation and propagation e.g. the possibility of crack deflection in the interfaces. The fact that the observed crack deflection modes are more numerous in ternary than in binary eutectics is in good agreement with the improvement of the fracture toughness from the individual constituents, to the binary eutectics and to the ternary eutectics. Concerning the creep strain rates of the ternary eutectics, it should be noted that the behaviour of the $Al_2O_3$-YAG-$ZrO_2$ and $Al_2O_3$-GAP-$ZrO_2$ eutectics is similar to that of the corresponding binary eutectics whereas that of the $Al_2O_3$-EAG-$ZrO_2$ eutectic is lower. The TEM examinations have evidenced plastic deformation of the various phases; furthermore, the different deformation modes thus observed are in good agreement with the stress exponents and activation energies experimentally determined. This better knowledge of the behaviour of DSE ceramics subjected to thermomechanical loadings has led to the development of a specific Bridgman furnace to produce large crystals and turbine blades. New eutectic compositions without $Al_2O_3$ phase will be investigated to improve the resistance to high temperature water vapor corrosion.

## ACKNOWLEDGEMENTS

The authors would like to thank M. Raffestin (FEG-SEM investigations), D. Boivin (EBSD studies), Dr. F. C. Lissalde (Bridgman furnace, Cyberstar) and Prof. J. Crampon for their kind cooperation and fruitful discussions. Dr. L. Perrière would also like to thank the French Defence Research Organization (DGA) for his Doctorate Scholarship.

## REFERENCES

[1] Waku Y., Nakagawa N., Wakamoto T., Ohtsubo H., Shimizu K. and Kohtoku Y., A ductile ceramic eutectic composite with high strength at 1873K. *Nature,* 1997, **389**, 49-52.

[2] Waku Y., Nakagawa N., Wakamoto T., Ohtsubo H., Shimizu K. and Kohtoku Y., High temperature strength and stability of unidirectionally solidified $Al_2O_3$/YAG eutectic composite. *J. Mater. Sci.*, 1998, **33**, 1217-1225.

[3] Gouadec G., Colomban Ph., Piquet N., Trichet M. F. and Mazerolles L., Raman/$Cr^{3+}$ fluorescence mapping of a melt-grown $Al_2O_3/GdAlO_3$ eutectic. *J. Eur. Ceram. Soc.*, 2005, **25**, 1447-1453.

[4] Piquet N., Microstructures interconnectées dans des eutectiques à base d'oxydes réfractaires élaborés par solidification dirigée. *Doctorate thesis*, Univ. Paris XII, 2006.

[5] Mazerolles L., Piquet N., Trichet M. F. and Parlier M., Microstructures and interfaces in melt-growth $Al_2O_3$-$Ln_2O_3$ based eutectic composites. *Adv. Sci. Techn.*, 2006, **45**, 1377-1384.

[6] Mazerolles L., Piquet N., Trichet M. F., Perrière L., Boivin D. and Parlier M., New microstructures in ceramic materials from the melt for high temperature applications, *Aerospace Sci. Techn.*, 2008, **12**, 499–505.

[7] Perrière L., Valle R., Mazerolles L. and Parlier M., Crack propagation in directionally solidified eutectic ceramics, *J. Eur. Ceram. Soc.*, 2008, **28**, 2337–2343.

[8] Mazerolles L., Perrière L., Lartigue-Korinek S., Piquet N. and Parlier M., Microstructures, crystallography of interfaces and creep behavior of melt-growth composites, *J. Eur. Ceram. Soc.*, 2008, 28, 2301–2308.

[9] Perrière L., Elaboration par solidification dirigée et comportement mécanique de céramiques eutectiques à base d'oxydes réfractaires. Rôle de la microstructure sur la fissuration et la déformation plastique à haute température. *Doctorate thesis*, Univ. Paris-Est, 2008.

[10] Peña J. I., Larson M., Merino R. I., de Francisco I., Orera V. M., Llorca J., Pastor J. Y., Martín A. and Segurado J., Processing, microstructure and mechanical properties of directionally-solidified $Al_2O_3$-$Y_3Al_5O_{12}$-$ZrO_2$ ternary eutectics, *J. Eur. Ceram. Soc.*, 2006, **26**, 3113-3121.

[11] Heuer A.H., Oxygen and aluminum diffusion in $\alpha$-$Al_2O_3$: How much do we really understand ?. *J. Eur. Ceram. Soc.*, 2008, **28**, 1495-1507.